A Conceptual Design for an Exoplanet Imager

David C. Hyland*, Jon Winkeller, Texas A&M University, College Station, Texas, 77843-3126; and Students of the Electromagnetic Sensing for Earth-Bourne Imaging class offered at Texas A&M in the Spring 2006 semester: **Project Manager:** Robert Mosher**; Assistant Project Manager:** Anif Momin**, Deputy Assistant Project Manager:** Gerardo Iglesias**; Mission Scientist:** Quentin Donnellan**, System Architecture Team:** Jerry Stanley, Storm Myers, William G. Whittington, Taro Asazuma, Gerardo Iglesias, Kami Slagle**; Optical Payload:** Lindsay Newton, Scott Bourgeois, Donny Tejeda, Brian Young**; Trajectory and Propulsion:** Nick Shaver, Jacob Cooper, Dennis Underwood, James Perkins, Nathan Morea**; Power and Thermal:** Ryan Goodnight, Aaron Colunga, Scott Peltier, Zane Singleton, John Brashear**; Structures and Materials:** Ronald McPherson, Winston Guillory, Sunil Patel, Rachel Stovall, Ryall Meyer; **Budget and Scheduling;** Patrick Eberle, Cole Morrison, Chun Yu Mong

ABSTRACT

This paper reports the results of a design study for an exoplanet imaging system. The design team consisted of the students in the "Electromagnetic Sensing for Space-Bourne Imaging" class taught by the principal author in the Spring, 2005 semester. The design challenge was to devise a space system capable of forming 10X10 pixel images of terrestrial-class planets out to 10 parsecs, observing in the 9.0 to 17.0 microns range. It was presumed that this system would operate after the Terrestrial Planet Finder had been deployed and had identified a number of planetary systems for more detailed imaging.

The design team evaluated a large number of tradeoffs, starting with the use of a single monolithic telescope, versus a truss-mounted sparse aperture, versus a formation of free-flying telescopes. Having selected the free-flyer option, the team studied a variety of sensing technologies, including amplitude interferometry, intensity correlation imaging (ICI, based on the Brown-Twiss effect and phase retrieval), heterodyne interferometry and direct electric field reconstruction. Intensity correlation imaging was found to have several advantages. It does not require combiner spacecraft, nor nanometer-level control of the relative positions, nor diffraction-limited optics. Orbit design, telescope design, spacecraft structural design, thermal management and communications architecture trades were also addressed. A six spacecraft design involving non-repeating baselines was selected. By varying the overall scale of the baselines it was found possible to unambiguously characterize an entire multi-planet system, to image the parent star and, for the largest base scales, to determine 10X10 pixel images of individual planets.

Keywords: Exoplanets, imaging, interferometry, entry pupil processing, optical heterodyne, intensity correlation

1. INTRODUCTION

The vision for space exploration has rallied behind a drive to understand the origins of life and to prove whether or not it exists elsewhere in the universe. Among the efforts to explore these questions are many interplanetary missions that look for evidence of past or present life by searching for spectroscopic evidence of atmospheric constituents believed to be necessary for life to exist. Examples include water as well as other bio-markers such as carbon dioxide, ozone, methane and nitrous oxide. In recent years, inspired by a steady stream of exo-solar planet discoveries, search efforts have been extended beyond the solar system into the stellar neighborhood by means of powerful new telescopes. NASA has envisioned several projects to encompass these goals and to provide answers to some of these questions through planet finding telescope systems such as the Terrestrial Planet Finder (TPF) and the Space Interferometry Mission (SIM)[1-3].

* dhiland@tamu.edu; phone 979 862-2647; fax 979 845-6051

Techniques and Instrumentation for Detection of Exoplanets III, edited by Daniel R. Coulter
Proc. of SPIE Vol. 6693, 66930K, (2007) · 0277-786X/07/$18 · doi: 10.1117/12.732648

The following study envisions a system that builds upon the accomplishments of TPF and SIM to take the study of exo-solar planets to a new level. This paper assesses the feasibility of obtaining multi-pixel images of Earth-sized planets in the proximity of other stars and to compare some of the current technologies for planet detection and imaging. The results show that while planet imaging is a challenge, it is feasible with current technology.

2. REQUIREMENTS

The following requirements represent the top-level design focus for this project. Each requirement serves to narrow the scope of the design effort to increase the probability of the final concept's success and to ensure that the vision of the mission is fulfilled. As mentioned previously, a key element to this design is to support the continuing search for life on distant worlds. Therefore, the science goal is to search for life markers in the atmospheric constituents of exo-planets. For this task, the observing system must be capable of fairly high resolution spectroscopy. The verifiable observation of life-associated compounds in the exo-planetary atmosphere can then be used to generate scientific theories about the past or present existence of living organisms.

Examples of life markers include carbon dioxide (CO_2), ozone (O_3), and methane (CH_4).[1] Collecting light within a 7 to 17 μm wavelength would allow for an imaging system to determine whether or not the collected light contained the signatures for any of these substances. However, the absorption band for methane is very narrow in comparison to ozone and carbon dioxide and would require the imaging system to have a very fine sensitivity to wavelength. This translates directly to an increase in cost and complexity. Therefore, the wavelength requirement was enforced at 9 to 17 μm, ensuring that the system will be able to detect ozone and carbon dioxide, without having the spectral resolution to detect methane.

It was decided not to configure the imaging system to search for evidence of life on gas giants similar to Jupiter or Saturn, but rather to address terrestrial class planets. Further, we assume that life needs a minimum of thermal energy to exist, and Earth-size planets far removed from a star may not have adequate average temperature to support life. Likewise planets too close to a star are too hot to harbor life. Therefore, in addition to containing certain substances as evidence for life, the targeted planet should be of the terrestrial class and be in orbit within the habitable zone of its parent star. The habitable zone of a star is a range of orbits that contain all planets whose surface temperatures do not exceed 373 K or fall below 273 K. Knowing the star temperature, star radius, and orbit radius, an accurate approximation of planet temperature can be obtained. To reduce somewhat the difficulty of the problem, we define a terrestrial class planet as one having a radius approximately that of Earth.

The principal objective of this design is to conceptualize an imaging system that takes the next step beyond the planned TPF system by producing multi-pixel images of identified exo-planets. The quantitative requirement that has been set for this project is to produce a 10 by 10 pixel image of the target planet. Images would look similar to Figure 1 below. Another self-imposed requirement is to design a system that will collect light with a signal-to-noise ratio (SNR) greater than or equal to 10.

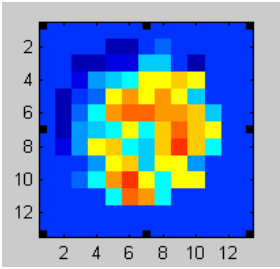

Figure 1: Sample Image Quality[3]

To limit the size and complexity of the imaging system, a specific range of stars needed to be established. Within 10 parsecs there are over 300 unique star systems, which is more than enough for several years of imaging missions. Moreover, detecting planets within 10 parsecs requires a baseline distance on the order of 2-3 km which is certainly an achievable goal for a space based imaging system. Therefore, it was decided that the limit to the range of

stars would be set at 10 parsecs. Additionally, this system will only focus on gathering light from M and K class star systems. For the brighter stars (including the Sun, a G class), the ratio of star brightness to planet brightness is so great that it would be extremely difficult to image any Earth-size planets orbiting that star, and detection alone would be a challenge. Even for M and K class stars, the star brightness is much greater than planet brightness, but it is significantly less than the ratio for higher spectral class stars and does somewhat alleviate the starlight nulling task. Furthermore, M and K class star constitute over 80% of the total population of stars in our galaxy. It therefore makes sense to focus not only on dimmer stars (easier to detect planets) but also on those which make up the majority of all known stars. The following is a list which reviews all of the top level requirements which will guide the design of this imaging system:

- Collect light within 9.0 to 17.0 μm wavelength range
- Target terrestrial planets (down to 1 Earth radii)
- Target planets in orbit within the habitable zone of parent stars
- Produce a 10 by 10 pixel image of target planet
- Achieve a signal-to-noise ratio (SNR) of at least 10
- Limit target range to a 10 parsec distance
- Limit star focus to M and K class stars

3. TELESCOPE SELECTION

A telescope design and arrangement capable of meeting the mission imaging requirements was chosen. The decision was primarily based upon size, weight, and cost. Several different types of telescopes and arrangements were considered, including the following options: singe telescope, monolithic, sparse aperture, multiple telescopes, free flying, and truss structures.

Single telescopes were a reasonable consideration because they are of familiar design. There were two types of single telescopes considered - monolithic and sparse aperture. The first consideration was the monolithic design, or in other words, a large telescope with a single, fully filled-in primary mirror. While this may seem to be a simple option, a monolithic telescope capable of imaging terrestrial sized planets up to 10 parsecs away would be continent-sized. Building such a telescope on the ground is completely infeasible, not to mention the unthinkable payload size to launch into space. Additionally, the surface accuracy required would make this option prohibitively expensive.

The second type of single telescope considered was the sparse aperture design which allows for the same angular resolution of a very large monolithic telescope, but uses only a few strategically placed mirror "spangles" to cut down on the weight and cost of the telescope. However, the diameter of the spangle arrangement must still be the same as the diameter of the mirror of a monolithic telescope, which leads to very limited, if any, launch options. In theory, the structure supporting the spangles could be folded into a compact form before launch and deployment, but not enough to easily fit into an existing rocket. Also, the structure would then to be deployed back into its operational shape and perform up to the mission requirements.

Since single telescopes do not provide any viable options, multiple telescope interferometers were investigated. There are two main types of these systems, a truss arrangement, and a free-flying configuration. The truss structure is a group of small telescopes attached by a frame which will work as a light collecting group to image the planets. This design provides for limited, but precise baselines that are constantly maintained very accurately. However, the truss structure makes the telescope system very large and launching is once again a problem. Cost is another disadvantage for this arrangement because it would be prohibitively expensive to assemble the telescope-truss structure in space, which is the only option for very long baselines.

The multiple telescope free flying arrangement was chosen as the best option for accomplishing the mission objectives. This design calls for multiple "small" telescopes (small when compared to the monolithic case) to be placed into a common orbit around the Earth in a strategically arranged group referred to as a "string of pearls." The arrangement allows for long baselines, but maintaining them within a specified accuracy becomes the primary challenge. However, for the chosen imaging method (to be discussed), the required baseline accuracy is on the order of a kilometer, which is attainable for this arrangement. Because this design only requires relatively small telescopes and no additional

truss material, it is the least expensive option, and most importantly, it can be launched in vehicles that are currently available.

4. IMAGING METHODS

The purpose of this section is to discuss the imaging methods available to this design as well as the justification for selecting intensity correlation imaging. The four methods considered included heterodyne interferometry, electric field reconstruction, amplitude interferometry, and intensity correlation imaging (based on the Hanbury Brown-Twiss effect).

Electric Field Reconstruction: [5-9]

The gathered beam of is gated into a sequence of brief pulses, and split into two parts. One part is spectrally sheared, meaning the frequency is shifted by a given value for the entire signal. After the shearing has occurred, the two beams of light are recombined onto a spectrograph. Spectral results yield the Fourier transform of each pulse. One of the limitations of this method is that of all the imaging choices considered, electric field reconstruction is the most complex and has only been proven to work for nearly coherent sources. In particular, the signal-to-noise ratio (SNR) for this imaging type is low.

Heterodyne Interferometry: [10-13]

Light gathered by each telescope is correlated with a local laser beam to produce a down-converted version of the incoming signal. The much lower frequency output signals from all telescopes are sent via RF links to some convenient place where the correlations among the signals are determined. The resulting data is then used to obtain the mutual coherence values for all pairs of collecting telescopes. The by inverse Fourier transformation the image is computed. The limitations of heterodyne interferometry include the fact that it requires multiple lasers of varying frequency for the ultimate coherence reconstructions. It also requires diffraction limited optics whose relative positions must be known to within a fraction of a wavelength for accurate measurements. The main source of noise is the noise inherent in light from vacuum state fluctuations.

Amplitude Interferometry: [14]

In this mainstream approach, the light collected by each telescope is split sufficiently many times and each sub-beam is propagated to a combiner device where it is combined with a sub-beam from another telescope and placed on a photodetector. Characteristics of the interference pattern observed by each combiner detector indicate the complex value of the mutual coherence for the locations of the corresponding pair of telescopes. Based on the mutual coherence measurements, the source image can be determined. Limitations of amplitude interferometry include the requirement of diffraction limited optics with relative telescope positions to be known and controlled to within a fraction of a wavelength. Because each separate pair of telescopes within a baseline must have their light beams correlated, each telescope must split its beam to be sent to combiners. This beam splitting and the large number of elements required for routing optics produce substantial signal loss, especially for more than two telescopes. There will be a combiner for each pair of telescopes and this necessitates a sizable number of additional spacecraft. Amplitude interferometry is very sensitive to starlight, so nulling is required for this method. To meet this requirement, each telescope must be replaced with a nulling pod. An example of a five telescope baseline would require using amplitude interferometry can be seen in Figure 2.

Intensity Correlation: [15-22]

Each light collecting telescope puts its light beam on a photodetector whose output is high-pass filtered and the resulting signal is communicated to some convenient location. The various measurements of intensity fluctuation are multiplied and time averaged to give estimates of the cross correlations of the intensity fluctuations observed at all pairs of telescopes. The basis of the Hanbury Brown-Twiss effect is that these intensity fluctuation cross correlations are proportional to the magnitudes of the mutual coherence values. The coherence phases can be either reconstructed from over-sampling and phase retrieval algorithms or deduced from triple or higher order correlations. Some well-known advantages are that combiner spacecraft are completely eliminated; nanometer-level control and optics measurement are not needed; light collecting optics are crude light buckets, not expensive, diffraction-limited telescopes; and the signal losses encountered in amplitude interferometry are absent. The latter feature means that the method's SNR increases indefinitely with the number of collecting apertures and the distances between telescopes can be arbitrarily large (hence

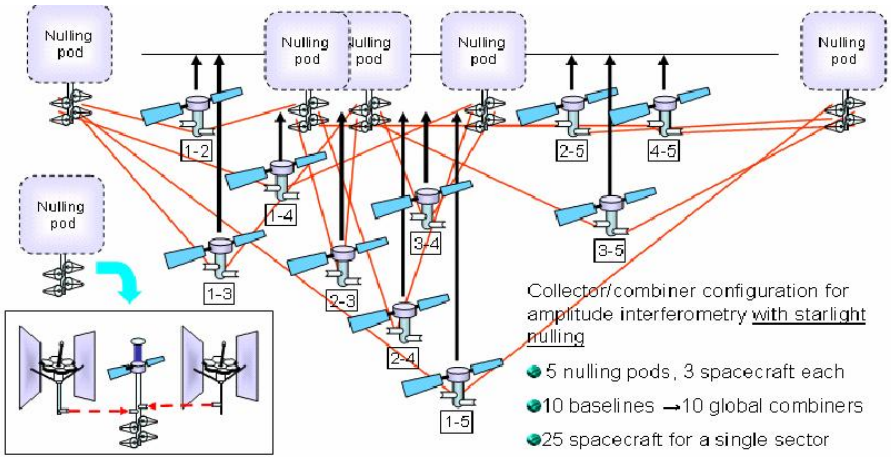

Figure 2: Baseline Using Amplitude Interferometry

almost any angular resolution can be attained). The biggest limitation of this method is its very small intrinsic sensitivity,.since it uses an effect that is second-order in the intensities. This drawback can be partially mitigated, however, by the use of large (cheap) collecting apertures, relatively long averaging times, and multiple frequency channels

The limitations of electric field reconstruction and heterodyne interferometry are prohibitive for the design. Of the two remaining options (namely intensity correlation and amplitude interferometry), further analysis must be conducted in order to determine which option will work the best. The comparison criteria include signal-to-noise ratios and the complexity of baseline geometry.

The required signal-to-noise ratio must be at least ten in order to accurately discern the image within the noisey data. Figure 3 contains the SNR equations for amplitude interferometry and intensity correlation, each with and without starlight nulling.[21]

Figure 3: SNR equations for Amplitude Interferometry and Intensity Correlation

	Amplitude Interferometry	Intensity Correlation
With Nulling	$\mu_f \sqrt{\frac{1}{2} N \tau_{opt} n_p \Delta\nu T}$	$n_p \sqrt{\frac{1}{2} N (N-1) \Delta\nu_d M_c T}$
Without Nulling	$\mu_f \sqrt{\frac{1}{2} N \tau_{opt} \Delta\nu T \frac{n_p^2}{n_s}}$	$n_p \frac{n_P}{P n_S} \sqrt{\frac{1}{2} N (N-1) \Delta\nu_d M_c T}$

μ_f	Losses associated with optics
τ_{opt}	Losses associated with beam splitting and beam transport
$\Delta\nu$	Frequency range of light collected
$\Delta\nu_d$	Frequency bandwidth of photo detector
M_c	Number of frequency channels
T	Averaging Time
n_p	Number of photons received from the planet per Hz per second
n_s	Number of photons received from the star per Hz per second
N	Number of Telescopes
P	Partial coherence factor ($\cong 10^{-3} to\ 10^{-5}$)

Due to the signal losses associated with amplitude interferometry, the SNR will drop with a sufficient increase in the number of telescopes. With amplitude interferometry, n_p in the "with nulling" case is replaced by the term n_p^2/n_s for the "without nulling case." The value of n_p is small when compared to n_s so without nulling, the SNR drops off considerably. For intensity correlation, the SNR increases with increasing number of telescopes. The reduction in SNR when starlight is not nulled is mitigated by the partial coherence effect (see below). To compare SNR values from the given equations, results were calculated for a possible star-planet system at ten parsecs for a two telescope case and a twenty telescope case. A summary of the data is provided in Table 1 below.

Table 1: Comparison of SNR values for different cases (Note: Approximate averages are presented because the SNR varies over the selected wavelength range.).

Number of Telescopes	Intensity Correlation SNR	Amplitude Interferometry SNR
2	1	300
20	15	10^{-6}

For the two telescope case, amplitude interferometry is the better option, but due to other design constraints, the number of telescopes needed is on the order of twenty. For twenty telescopes, the signal losses associated with beam splitting and transport reduce the SNR to well below ten for amplitude interferometry. Intensity correlation, however, achieves an acceptable SNR for this number of telescopes.

Lastly, baseline geometry complexity was considered. For amplitude interferometry, a combiner is needed for each telescope pair, and each spacecraft will need to be on the same orbit to maintain distances between spacecraft. The baseline geometry of intensity correlation has a much simpler configuration because combiners are unnecessary, and the relative distances do not need to be maintained as accurately as those in amplitude interferometry. As a result, intensity correlation was chosen as the imaging method for this design because it can meet the requirements for SNR without an overly complex baseline geometry.

5. LIGHT COLLECTOR DESIGN

The High Accuracy Reflector Development (HARD) deployment scheme was chosen for the design because it best fulfilled the surface area, stowed length, and manufacturing requirements. The HARD program originated at NASA in 1981, and the well-developed concept has been incorporated in many space vehicles including NASA's Terrestrial Planet Finder[2]. The configuration consists of 18 hexagonal panels, each made of an optical glass [ZERODUR (Schott Glass) or Corning ULE Glass] that has a low coefficient of thermal expansion.These panels are able to rotate and stack themselves vertically which makes a compact form suitable for the mission.

The reflector uses a rotational translational joint (RTJ) to move each panel into its deployed position. The stowed panels are initially stacked inside the payload area while mechanical restraints support the stack. The center panel is the bottom panel in the stock. The first maneuver in the deployment sequence is for the stack to be lifted up off the bottom panel to provide clearance after the restraints are released[29]. The entire stack then rotates about the RTJ using a turntable to position the next panel in the stack in its deployed position[30]. The stack lowers down, and the next panel locks edge-to-edge to the center panel. This process continues until all of the panels are in place. A ball-cone latch mechanism locks each panel into place for precision alignment. After all panels are in place, the RTJ is removed from the system kinematically[30]. Figure 4 demonstrates the deployment sequence.

Additionally, the stowed configuration was desirable because it is independently stable, meaning no additional hardware is required to stabilize the spacecraft. Also, the hexagonal panels fit together in a way to minimize the area loss due to edge affects[30].

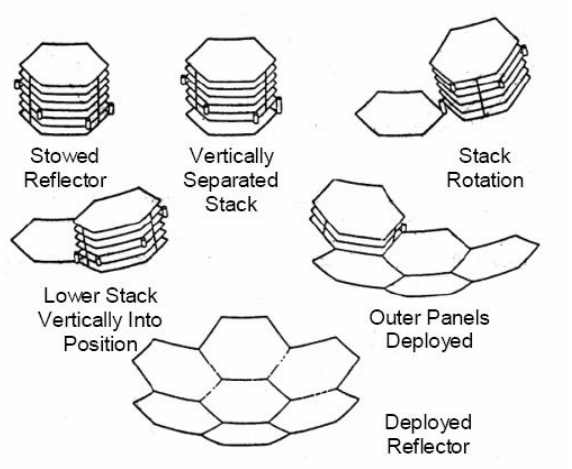

Figure 4: Light collector deployment sequence

6. LAUNCH & ORBIT LOCATION

A launch vehicle is required to place the satellites into space. First, a table of launch vehicles was compiled from lists of available published data. Based on a rough payload mass estimate of 5,000 kg and a minimum payload stowed diameter of 3 meters, the search was refined until a selection could be made. Taking cost and practicality into consideration, the Delta IVM rocket was chosen.

It was known that the satellites could be placed at different orbits around the earth, or moon if desired. The goal then became a matter of determining the most efficient orbit for the light collectors given the system requirements. The trade study options were analyzed assuming that the orbits consisted of four strings of six satellites, each at 45 degree increments apart. Such an arrangement primarily affected the time required to sweep out a complete Modulation Transfer Function (MTF) coverage such that the desired SNR was attained. The MTF is defined as the ratio of estimated intensity to true image intensity, and it serves as a measure for the imaging system's performance. In other words, the MTF describes the input/output behavior of the imaging system.

Low Earth orbit was the first trade option researched because it is known to have the lowest ΔV for orbit insertion. With the launch vehicle Ariane 5, as with many others, there would be no additional ΔV to insert the satellites into orbit, and this would allow for a maximum payload mass of 11,000 kg. Another benefit of LEO is that the MTF would be filled in approximately 20 minutes due to the short orbital period. However, the main factors that ruled out LEO included atmospheric drag and high Earth irradiance. Since the fully-deployed light collectors would be 15 meters in diameter, the atmospheric drag on the satellites would become a concern and require more fuel to keep the spacecraft in orbit. Additionally, the large amount of sunlight reflected from Earth to the satellite would cause undesirable heating of the optics.

Geosynchronous orbit was found to be the most efficient placement for the satellites because not only does it have a relatively short period (24 hours, which allows the MTF to be covered in approximately three hours), but atmospheric drag is not an issue. Additionally, the ΔV required for orbit insertion is relatively small which allows for a reasonably heavy payload to be placed into orbit.

Next, an orbit with twice the radius of GEO was considered. The main reason that twice GEO was not chosen was that it would require in excess of 50% more fuel than it would to put the satellite in a GEO orbit. The other important deciding factor was that it would take more than twice as long to sweep out a full MTF. Although this orbit experiences less of an Earth irradiance problem, it should also be noted that at GEO this effect could be dealt with by using sun shades (to be discussed further in the thermal analysis).

A lunar orbit was originally considered because of the short time required to produce a full MTF, as dictated by its short period. However, the benefit was not worth the cost of a much greater ΔV. The L2 point was also considered

as a solution for the Earth and Moon irradiance problem because it would be far away from both of these radiating bodies. However, when compared to GEO, this orbit required much more fuel and was not a practical solution. Therefore, based on the arguments presented in the preceding discussion, a geosynchronous orbit was chosen to best meet the requirements for the imaging system.

7. ORBIT DESIGN

Many options were available for configuring the orbit, each of which had a large effect on the performance of the imaging system. The purpose of orbit design is to evaluate the best option for the placement of the satellites and how to maintain them in orbit within the required tolerances.

The first configuration considered was a series of concentric orbits. This orientation involves placing satellites into several circular orbits with increasing altitudes. The design itself is simple, but it is rather complex for the imager to obtain the full MTF since each satellite would have a different orbital period. The time to obtain the full MTF would be half the orbit period of the longest orbit. A benefit with this configuration is that the orbital radius tolerance would be less than or equal to 1 km.

The next idea investigated was a "string of pearls" configuration, consisting of satellites grouped together in the same orbit. This was originally suggested by Hussein, Scheeres, and Hyland[4]. Interferometric observatories in earth orbit. Journal of Guidance, Control and Dynamics, Vol. 27, No. 2, pp. 297–301, 2004.
Multiple string groupings can be placed into the same orbit to reduce the required time to fill the MTF by a factor equal to the reciprocal of the number of strings added. This design is very simple, and the station-keeping tolerances required by the HB-T method are approximately 1 km.

Finally, a special kind of orbit known as a flower constellation was considered. The flower constellation is a design which involves placing satellites into critically inclined, compatible orbits. This method proved to be very complex to obtain a full MTF and satellite tracking was also an issue. For these reasons, this type of orbit configuration was ruled out. Figure 5 below illustrates each of the configurations in this trade study.

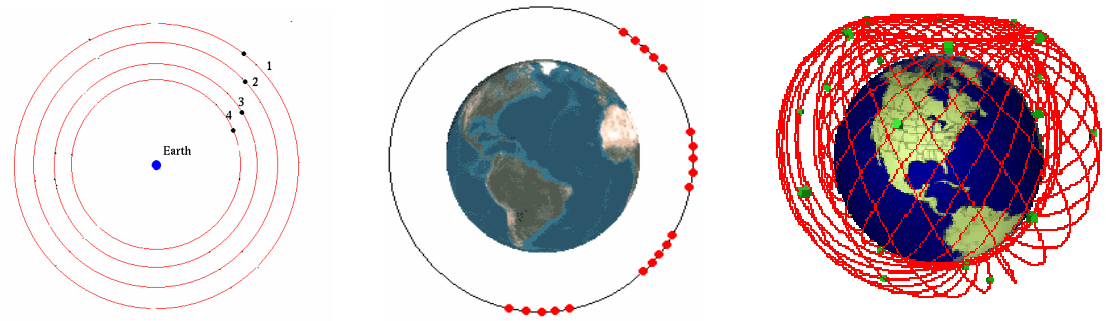

Figure 5: Possible design configurations: concentric, string of pearls, flower constellation

An optimized orbit configuration is desired to meet mission requirements for the lowest risk and cost. The MTF can be filled out by all three configurations. However, the time to fill out the MTF is driven by the orbits of the pair of satellites having the largest orbit radii. Placing additional satellites in lower orbits does not, in fact improve the rate of u-v coverage beyond what would be attained by adding more satellites at the maximum orbit radius. This tends to argue against the use of concentric orbits. Furthermore, the relative positions among spacecraft in concentric circular orbits are adversely effected by perturbations whereas in the string of pearls configuration, each satellite experiences similar disturbing forces and the effects are easier to manage.

For the reasons outlined above, the string of pearls was selected as the orbit configuration for the imaging system. The primary benefit for this arrangement is that it relies on passive maneuvering and only needs enough fuel to reach orbit and then serve station-keeping purposes. Passive maneuvering also allows for a greater lifetime at a lower cost when compared to orbits requiring active maneuvering for u-v plane coverage.

8. DATA PROCESSING & IMAGE CONSTRUCTION

A sequence of telescope-bearing spacecraft are distributed along the same GEO orbit as pictured in Figure 6. Nominally, the line of sight (LOS) vector is along the orbit normal. In this configuration, the vectors associated with MTF coverage make a complete rotation about the disc origin every half orbit.
The telescopes are spaced with the following three different length scales:

$$\begin{aligned} D_C &= \frac{2\pi}{8} r_{GEO} \\ D_{Pix} &= \frac{\lambda}{\theta_{Pix}}, \quad \theta_{Pix} \cong \frac{R_P}{10\bar{z}} \Rightarrow |\vec{u}| \cong \frac{1}{\theta_{Pix}} \\ D_P &= \frac{\lambda}{\theta_P}, \quad \theta_P \cong \frac{R_P}{\bar{z}} \Rightarrow |\vec{u}| \cong \frac{1}{\theta_P} \end{aligned} \tag{1.a-c}$$

where $\vec{u}$ is the wave vector in the Fourier domain (the 'u-v plane").There are four independent groups of spacecraft, as shown, distributed at a distance D_C along the common circular orbit. Note that light collected by two telescopes in different groups are not correlated; only data from within the same group are correlated. This serves to augment the rate of u-v coverage at the required SNR fourfold. D_{Pix} corresponds to the baseline required to resolve a single pixel, where the pixel size is roughly the required angular resolution. D_P corresponds to the picture frame size, i.e. the pixel size times the number of desired pixels on a side. In other words, this distance is comparable to the baseline required to just resolve the disk of the planet. If we take the Sun-Earth system as our guide, the baselines needed to resolve (1) the system (distinguish the planet from the star); (2) the disk of the star, and (3) the disk of the planet are separated by two orders of magnitude.

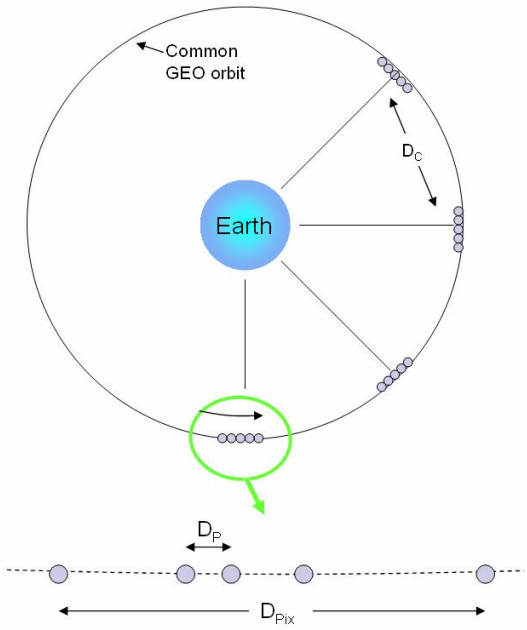

Figure 6: String of pearls imaging constellation

Next, Figure 7 describes the geometric conventions. The left part of the figure describes the orientation of one pair of light-collecting spacecraft in the plane normal to the LOS. The right side shows the geometry of the apparent relative position of the star and planet in the look-angle plane.

The mutual coherence function is given by

$$\Gamma(\vec{u}) = \Gamma_S(\vec{u}) + \Gamma_P(\vec{u}) \tag{2}$$

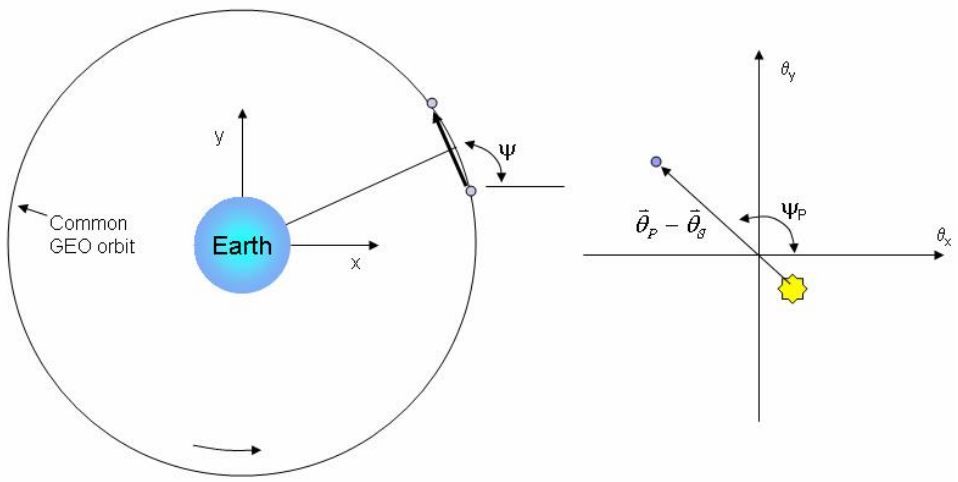

Figure 7: Orientation angle Ψ for two selected light collectors (left), and orientation angle Ψ_P for the apparent star/planet configuration (right).

where $\Gamma_S(\vec{u})$ is the coherence due to the star alone and $\Gamma_P(\vec{u})$ is the coherence due to the planet alone. These quantities are further defined by the expressions:

$$\Gamma_S(\vec{u}) = T_{av}\Delta\nu n_S\, \gamma_S(\vec{u}) \exp\left\{2\pi i\left(u\theta_{Sx} + v\theta_{Sy}\right)\right\} \tag{3}$$

$$\Gamma_P(\vec{u}) = T_{av}\Delta\nu n_P\, \gamma_P(\vec{u}) \exp\left\{2\pi i\left(u\theta_{Px} + v\theta_{Py}\right)\right\} \tag{4}$$

where

$\gamma_S(\vec{u})$	Normalized coherence function of the star when centered at the origin of the look angle plane
$\gamma_P(\vec{u})$	Normalized coherence function of the planet centered at the origin of the look angle plane
n_s	Number of photons from the star received by a single aperture per second, per Hertz
n_P	Number of photons from the planet received by a single aperture per second, per Hertz
$\Delta\nu$	Frequency band of radiation received by the detectors
T_{av}	Averaging time used for the cross-correlations of photodetector output fluctuations

Since Ψ is the angular orientation of one of the telescope pairs the wave vector associated with the coherence measurement is:

$$\vec{u}(\psi) = u\left[\hat{\mathbf{u}}\cos\psi + \hat{\mathbf{v}}\sin\psi\right], \quad u = |\vec{u}|. \tag{5}$$

In this analysis, it is assumed that the distance between any pair of spacecraft is maintained constant as the pair traverses the orbit. Therefore, for any pair of collectors, $\gamma_P(\vec{u})$ and $\gamma_S(\vec{u})$ are functions of u = constant and $\psi \in [0, 2\pi)$.

Now, let:

$$\overline{\gamma}_S(\vec{u}) = \rho_S(u,\psi)\exp\left(2\pi i\varphi_S(u,\psi)\right) \tag{6}$$

$$\overline{\gamma}_P(\vec{u}) = \rho_P(u,\psi)\exp\left(2\pi i\varphi_P(u,\psi)\right). \tag{7}$$

Using the above expressions, we can evaluate the magnitude of the coherence, which is the quantity actually measured via the Hanbury Brown-Twiss technique. Neglecting terms of second-order and higher in the ratio of the planet to the star flux, we get:

$$\left|\Gamma_{Signal}(\vec{u})\right| = T_{av}\Delta\nu\left[\begin{array}{l}\overline{n}_S\rho_S(u,\psi) \\ +\overline{n}_P\rho_P(u,\psi)\cos\left(2\pi\left[u\left|\vec{\theta}_P - \vec{\theta}_S\right|\cos\left(\psi - \psi_P\right) + \varphi_P(u,\psi) - \varphi_S(u,\psi)\right]\right) + O\left[\left(\frac{\overline{n}_P}{\overline{n}_S}\right)^2\right]\end{array}\right] \tag{8}$$

This expression is reminiscent of a heterodyne process in which the star light plays the role of the local oscillator. Note that we have not, so far, mentioned starlight nulling. This would be an inconceivable oversight for an amplitude interferometry system. But for an intensity correlation imaging stystem, we would argue that we can do without nulling as follows.

As a result of Terrestrial Planet Finder studies, $\vec{\theta}_P - \vec{\theta}_S$ and $\overline{n}_P$ will be known. Additionally, $\rho_S(u)$ and $\varphi_S(u,\psi)$ will be determined from a preliminary star characterization process using baselines $\cong 1/\theta_{R_P}$. Owing to the disparity between the length scales of the longer-term stellar features and the length scales of the planet, this can be done so that the first term in (8) is determined to very high accuracy; at least to order $\left(\overline{n}_P/\overline{n}_S\right)^2$. Thus, in the planet imaging process, the "signal" is actually the second term on the right of equation (8), with $\varphi_S(u,\psi)$ already determined and the magnitude of this signal proportional to the planet brightness. If we were to null the star light, $\left|\Gamma_{Signal}(\vec{u})\right|$ would be the magnitude of the planet coherence alone, which again has magnitude equal to the planet brightness. There is thus no gain in effective signal strength to be obtained by starlight nulling. Moreover this conclusion is further reinforced by the effects of partial coherence on the estimated coherence magnitude. Our apertures are large enough to easily resolve the typical star, but not the planet. Due to the partial coherence factor, the contribution of starlight to the measured coherence will be substantially reduced, as pointed out in a companion paper to this conference[31]. The HBT approach intrinsically offers a corongraphic effect by virtue of partial coherence.

To describe the planet imaging process, first define T_E such that:

$$\frac{2\pi}{\Omega} >> T_E >> \frac{2\pi/\Omega}{u\left|\vec{\theta}_P - \vec{\theta}_S\right|} \tag{9}$$

Then, for each baseline distance, accumulate the following running averages as Ψ progresses from 0 to 2π.

$$\begin{aligned} S_C &= \frac{-\Omega}{2T_E}\int_{t-T_E}^{t} d\tau \frac{\operatorname{sgn}\left(\overline{\gamma}_S(u)\right)}{\overline{n}_P T_{av}\Delta\nu}\left[\left|\Gamma_{Meas}(\vec{u})\right| - T_{av}\Delta\nu\overline{n}_S\rho_S(u)\right]\cos\left[2\pi\left(u\left|\vec{\theta}_P - \vec{\theta}_S\right|\cos\left(\psi-\psi_P\right)\right)\right]\left(\sin\left(\psi-\psi_P\right)\right) \\ S_S &= \frac{-\Omega}{2T_E}\int_{t-T_E}^{t} d\tau \frac{\operatorname{sgn}\left(\overline{\gamma}_S(u)\right)}{\overline{n}_P T_{av}\Delta\nu}\left[\left|\Gamma_{Meas}(\vec{u})\right| - T_{av}\Delta\nu\overline{n}_S\rho_S(u)\right]\sin\left[2\pi\left(u\left|\vec{\theta}_P - \vec{\theta}_S\right|\cos\left(\psi-\psi_P\right)\right)\right]\left(\sin\left(\psi-\psi_P\right)\right) \end{aligned} \tag{10}$$

Using the equations above, $\overline{\gamma}_P(u,\psi)$ is determined by

$$\overline{\gamma}_P(u,\psi) = S_C + iS_S \,. \tag{11}$$

Finally, performing the inverse Fourier transform of $\overline{\gamma}_P(u,\psi)$ produces $I_P(\vec{\theta})$, the image intensity.

Multiple planet systems have also been analyzed. One starts by imaging the planet with the largest apparent distance from its star. One can then construct a projection operator, the application of which nulls the contribution of the apparently outermost planet to $\left|\Gamma_{Meas}(\vec{u})\right|$. One then proceeds to image the next most distant planet and continues on in this way until the imaging of the apparently innermost planet is completed.

9. THERMAL MANAGEMENT

For this mission, the thermal environment helped drive the decision for the necessary type of orbit. Due to the low temperature requirement of the optics (<40 K), only orbits with low effective heating rates were considered. A trade study was performed to solve for the effective heating rates due to direct solar radiation, Earth irradiation, Earth albedo, Moon irradiation, and Moon albedo in LEO, GEO, 2GEO, Lunar and L2 orbits. The results are summarized below in Table 2. GEO, 2GEO, and L2 orbits are the most desirable from a thermal standpoint. Although 2GEO and L2 orbits have lower effective heating rates, the increased cost and lower mass more than offsets the slightly better thermal environment.

Table 2: Effective Heating Rate Trade Study*[23,25,26]

	LEO (700 km)	GEO (42k km)	2GEO (84k km)	Lunar (700 km)	L2
Direct Solar (W)	109.68	109.68	109.68	109.68	109.68
Earth IR (W)	38.83	0.82	0.24	0.01	0.00
Earth Albedo (W)	30.98	0.48	0.04	0.00	0.00
Moon IR (W)	0.02	0.02	0.03	32.01	0.00
Moon Albedo (W)	0.00	0.00	0.00	1.21	0.00

Two configurations were studied to prevent heat build-up in the spacecraft to help achieve the optics temperature requirement. The first configuration was a design that had been proposed by Northrop Grumman for the Next Generation Space Telescope (NGST), but had never been used in orbit[27]. It involves an omni-directional, inflatable sunshade which surrounds the telescope and extends from the base along the line of sight. In essence, it is an inflatable version of the telescope barrel for the Hubble Space Telescope. By making the sunshade long enough, light will only be able to hit the reflector from a narrow range of angles, preventing stray light from contaminating the images. It also blocks incoming light from the Earth and Sun without having to change its orientation. However, deploying this structure would be difficult for the reflector design that is being considered. Currently, the reflector is a folding mirror that unfolds in orbit. Placing a structure to deploy the sunshade around these unfolding panels would be extremely difficult. This is because the reflector has no fixed outer ring, but grows as it unfolds. Another issue is that the surface area of the sunshade is sensitive to the diameter of the telescope. By changing the telescope diameter by 1 meter, the surface area will increase by $3.14m^2$. Also, since it has never been tested or flown the TRL of this concept is very low (approximately a 4).

The second configuration considered is a modification of a proven design, based upon NASA's Inflatable Sunshade in Space (ISIS) Experiment for the NGST[28,29]. This design uses two flat inflatable sunshades, one each for the Earth and Sun, to block incoming light. The sunshades are suspended on booms from the bottom hub of the spacecraft. By placing the sunshades on booms, the deployment of the reflector will have no effect on the deployment of the sunshades. Also, having flat sunshades makes them less sensitive to reflector size. Another positive aspect is that an inflatable sunshade of this design has been built in a laboratory. A definitive drawback, however, is that the sunshades must be constantly reoriented as the spacecraft orbits around the Earth. This means there must be a mechanism to rotate the sunshades without changing the orientation of the telescope.

Both the sunshades and support booms are inflatable. The booms are made of an uncured thermoset composite laminate that is inflated by an inert gas. Solar heating will cause the composite to set and harden. Deploying the booms will cause the membranes to unfold to their final position. Once in the deployed position, the sunshades can be rotated about the spacecraft by electric motors in the spacecraft hub.

Due to issues pertaining to deployment, the flat sunshade configuration was chosen for the design. Each sunshade is 153 m^2 of 0.013 mm-thick silvered aluminum oxide and multi-layer insulation (MLI). A majority of the sunshade mass comes from the support booms because it must contain the gas that is used to inflate the sunshade. After a 35% margin is added to the final mass, a rough figure of 185 kg was calculated for the complete sunshade system.

10. POWER SYSTEM

The overall size and mass of the power subsystem is a function of the power requirements for all of the onboard electronics during their peak usage. In this preliminary design, the exact specifications of all the required electrical components onboard are not precisely defined. Thus in order to determine the overall power requirements, previous scientific spacecraft with similar missions were analyzed. Referencing a recent study regarding power usage trends for

* Calculations based on references 24 and 26. Geometry and materials (specifically absorptivity and emissivity) were included and based upon the sunshade design described in the next section.

spacecraft missions[24] and by comparing our anticipated required imaging electronics with those onboard previous astronomical spacecraft, the overall power requirement was estimated to be approximately 1000 W. Once the overall power consumption was estimated, the solar cell array and batteries were sized accordingly.

The purpose of the onboard batteries are to provide extra power during times when the input power from the solar panel array is less than the power required by the onboard electronics. The desired orbit was analyzed to determine the amount of time spent in an eclipse. A GEO orbit consists of approximately 90 eclipse days per year, with the maximum eclipse time not exceeding 72 minutes. Using this information and taking into account the desired lifetime of the spacecraft, the cycle life of the batteries will be no more than 1000 cycles. The maximum allowed depth of discharge (DOD) for batteries is a function of cycle life and battery chemistry. For this mission as a baseline it was assumed that nickel cadmium batteries will be used. According to previous battery research[26] for nickel cadmium chemistry with a cycle life of 1000, the maximum DOD is approximately 60%. Considering a maximum eclipse of 72 minutes, a minimum charge time (time till next eclipse) of 22 hours and 48 minutes, and with a DOD of 60%, the required battery capacity is 2400 WHr. To account of the simplicity of this analysis the estimate includes a 50% contingency in required battery capacity.

The solar panel array must be sufficiently sized such that during a maximum eclipse of 72 minutes, and thus a corresponding minimum charge time of slightly less than 23 hours, the panels will produce enough power for all the onboard electronics while also providing enough power to recharge the battery in preparation for the next eclipse. With an estimated power consumption of 1000W, and the battery configuration discussed above discharged by 60%, the required output of the solar cell array must be at least 1330 W. With the required output determined, the efficiency of the solar panels over the course of the entire mission was considered. For a GEO orbit with a flat silicon solar array and a corresponding worst-case sun angle of 23.5 degrees between equatorial and ecliptic planes, the power output at the beginning-of-life is 143 W/m^2. The life degradation of the panels was then calculated considering the desired satellite lifetime to be 17%. Taking this into account, the panel end-of-life output will be 118 W/m^2. Sizing the panels based off the end-of-life power output to provide the required total output of 1330 W yields a required solar panel array area of 11.3 m^2.

The total required power for all the onboard electronics was estimated by comparing previous spacecraft with similar missions. The batteries and solar panels were sized accordingly while accounting for a GEO orbit and the degradation of the components over the lifetime of the mission. From these estimates the overall size, mass, and cost of the entire power subsystem were determined (see Table 3). A parametric cost estimation was performed which was a function of the overall subsystem mass and the beginning-of-life power output of the solar panel array[27].

Table 3: Power System Estimates

Power Required	1000 W
Power System Mass	221 kg
Solar Array Area	11.3 m^2
Cost Estimate	$24M

11. SUMMARY

The purpose of this study was to design a mission concept for following up the planet detection discoveries of NASA's Terrestrial Planet Finder (TPF) with detailed images of the newly discovered planets. The mission requirements set forth from the beginning drove the choices presented in this design. Figure 8 illustrates the final configuration of one spacecraft sub-group of the conceptual design. Although some of the major decisions resulted from sub-level requirements, a few came directly from the top-level requirements. For instance, the infrared band requirement of 9-17 microns, which increases the chances of finding life-supporting planets, led to a space-based system design. Another major decision that came from the top-level requirement was using Hanbury-Brown Twiss intensity correlation technique without starlight nulling to achieve a 10x10 pixel image. Additionally, achieving a signal-to-noise ratio of at least 10 would require dilation of strings of the light collectors and long averaging time for fewer then five light collectors. However, as the number of light collectors increases above five, the averaging time continues to drop and dilation would no longer be needed (except for extreme off-angle viewing). Therefore, for the current study, the design

decision was that six light collectors be launched initially. Another major decision based on the top-level requirements was limiting the imaging of planets to those similar in size to Earth (down to three times the radius of the Earth) and focusing on planets satisfying the habitable zone requirement. These design choices along with the sub-level choices from this study demonstrate that the imager design is feasible with current technology.

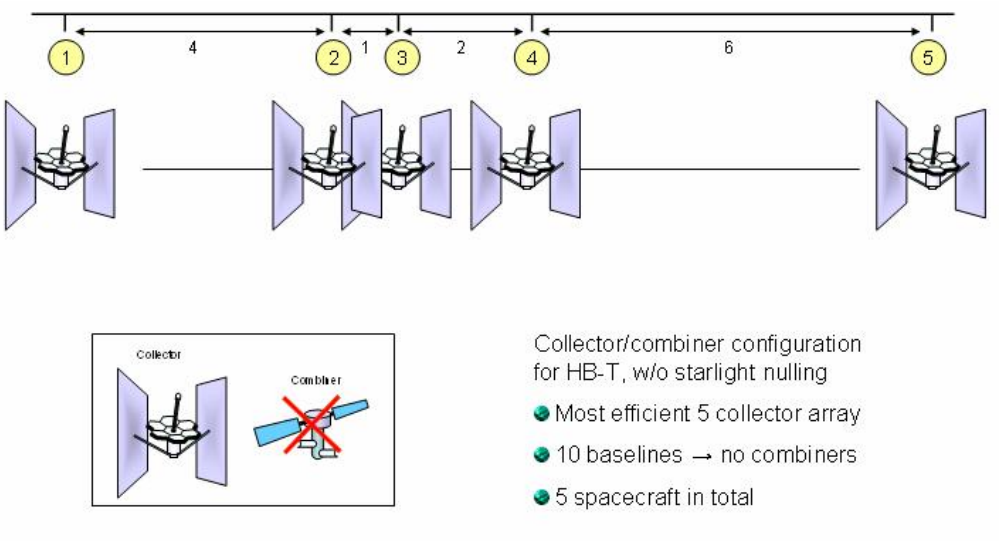

Figure 8: Final configuration of the conceptual design

REFERENCES

1. Beichman, Charles Ph.D., An Integrated Approach to Finding Planets – From Kepler to Terrestrial Planet Finder-1, 9 March 2005
2. "Terrestrial Planet Finder." JPL Publication 99-3, May 1999. <http:/tpf.jpl.nasa.gov/library/tpf_book/index.html>.
3. "Images." Spitzer Space Telescope. Jet Propulsion Laboratory. 04 Apr. 2006 <http://www.spitzer.caltech.edu/>.
4. I. I. Hussein, D. J. Scheeres, and D. C. Hyland. "Interferometric observatories in earth orbit". Journal of Guidance, Control and Dynamics, Vol. 27, No. 2, pp. 297–301, 2004.
5. C. Iaconis, and I. A. Walmsley, "Spectral phase interferometry for direct electric-field reconstruction of ultrashort optical pulses", *Opt. Soc. Am.,* Jan. 1998.
6. T. I. Kuznetsova and I.A. Walmsley, "Reconstruction of temporal signals from nonlinear optical measurements", *Quantum Electronics,* 28 (8), 728-732, 1998.
7. C. Iaconis, and I. A. Walmsley, "Self-referencing spectral interferometry for measuring ultrashort optica pulses", *IEEE Jour. of Quantum Electronics,* Vol.35, No. 4, April, 1999.
8. L. Lepetit, G. Cheriaux, and M. Joffre, "Linear techniques of phase measurement by femtosecond spectral interferometry for applications in spectroscopy", *J. Opt. Soc. Am. B*, Vol.12, No. 12, December, 1995.
9. C. Dorrer, "Implementation of spectral phase interferometry for direct electric-field reconstruction with a simultaneously recorded reference interferometry", *Optics Letters,* Vol.24, No. 21, November, 1999.
10. C. H. Townes, *J. Astrophys. Astron.,*5, 111, 1984.
11. C. H. Townes et al. Proc. SPIE, 908, 3350, 1998.
12. M. Bester, W. C. Danchi, and C. H. Townes, Proc. SPIE, 40, 1237, 1990.
13. R. H. Kingston, in *Optical Sciences,* Vol.10, ed. D. L. MacAdam (New York: Springer),28, 1978.
14. A. Quirrenbach, "Optical Interferometry", *Annu. Rev. Astron. Astrophys.* 2001.39:353-401.
15. Brown, R. Hanbury and Twiss, R.Q.(1956a), *Nature* **177**, 27.
16. Brown, R. Hanbury and Twiss, R.Q.(1957a), *Proc. Roy. Soc. (London) A* **242**, 300.
17. Brown, R. Hanbury and Twiss, R.Q.(1958a), *Proc. Roy. Soc. (London) A* **248**, 199.
18. Brown, R. Hanbury, Davis, J. and Allen, L.R. (1967a), *Mon. Not. R. Astron. Soc.* 137, 375.
19. D.C. Hyland, "Extrasolar Planet Detection Via Stellar Intensity Correlation Interferometry", 35th Colloquium on the Physics of Quantum Electronics, Snowbird, Utah, January 2-6, 2005.
20. D. C. Hyland, "Exo-Planet Detection Via Stellar Intensity Correlation Interferometry, Techniques and Instrumentation for Detection of Exoplanets II, SPIE International Symposium on Optics & Photonics, SPIE paper no. 5905-37, 31 July – August 4, San Diego, California.

21. D. C. Hyland, “Entry Pupil Processing Approches for Exo-Planet Imaging, Techniques and Instrumentation for Detection of Exoplanets II, SPIE International Symposium on Optics & Photonics, SPIE paper no. 5905-27, 31 July – August 4, San Diego, California.
22. L. D. Millard and D.C. Hyland, “Simplifying Control of Interferometric Imaging Satellite Formations: Benefits of Novel Optical Architectures”, AAS paper AAS03-547, American Astronautical Society Conference, Big Sky, Montana, January, 2004.
23. Brown, Charles D. Elements of Spacecraft Design. Reston: The American Institute of Aeronautics and Astronautics, 2002.
24. Cyrus, Jilla D. Satellite Design: Past, Present, and Future. International Journal of Small Satellite Engineering, February, 1997.
25. Gilmore, David G. Spacecraft Thermal Control Handbook. El Segundo: The Aerospace Press, 2002.
26. Larson, Wiley J. and James R. Wertz. Space Mission Analysis and Design. El Segundo: Microcosm Press, 1999.
27. Lillie, Chuck. A Large Aperture Deployable Telescope for the Next UV/Optical Telescope (NHST). Northrop Grumman: 2003.
28. Sandy, Charles. Next Generation Space Telescope Inflatable Sunshield Development. ILC Dover: 2000.
29. Lillie, Charles F. Whiddon, William B. Deployable Optics for Future Space Observatories. The American Institute of Aeronautics and Astronautics, 2004.
30. Lindsay, Geoff. "NAVAIR Technology Needs Survey Document." NAVAIR. 25 Apr. 2002. <http://www.enviro-navair.navy.mil/TNS2001-08-01-01.NSF/0/a5893452279dcaab85256e9f0056d2d4>.
31. D. C. Hyland, “Calculation of Signal-to-Noise Ratio for Image Formation Using Multispectral Intensity Correlation”, Techniques and Instrumentation for Detection of Exoplanets III, SPIE International Symposium on Optical Engineering and Applications, SPIE paper no. 6693-23, 26-30 August , 2007 San Diego, California.